ISBN: 978-628-96613-1-6. ISSN: 2414-6390. Digital Object Identifier: https://dx.doi.org/10.18687/LACCEI2025.1.1.1089

3UPS Parallel Mechanism for Passive Rehabilitation of Lateral Ankle Sprains in Ball Sport Athletes

Dario Gonzalez-Dancourt[1]; Deyby Huamanchahua[1]
[1]*Universidad de Ingenieria y Tecnologia - UTEC, Department of Electrical and Mechatronics Engineering, Lima, Peru,* dario.gonzalez@utec.edu.pe, dhuamanchahua@utec.edu.pe

Abstract*– This work focuses on designing and developing a 3UPS parallel mechanism for passive rehabilitation of lateral ankle sprains in ball sport athletes. The study analyzes the high incidence of this musculoskeletal injury and its functional and social impact. The proposed mechanism seeks to accurately replicate the physiological movements of the ankle through the integration of advanced inverse kinematics methods and screw theory. The required ranges of motion were defined to ensure a proper and safe recovery. The results show that the mechanism fully achieves the physiological ranges required: dorsiflexion-plantarflexion from 30° to –20°, abduction-adduction from 10° to –10°, and eversion-inversion from 20° to –10°. Moreover, the workspace analysis demonstrated adequate coverage in both positional and orientational domains, with vertical displacements ranging from 0.01 m to 0.2717 m, and maximum achievable angles of ±61.00° for ψ, from 24.77° to –18.72° for θ, and ±22.35° for φ. Likewise, the singularity analysis initially revealed 22 critical position configurations and 44 for orientation, which were reduced to 12 and 14 after eliminating redundancies. Importantly, all singularities lie outside the effective workspace. This development provides an accessible, robust, and efficient solution for improving rehabilitation and preventing future complications such as chronic ankle instability.

Keywords*— 3UPS, ankle sprains, inverse kinematics, geometric method, screw theory.

I. INTRODUCTION

The growing prevalence of musculoskeletal disorders, such as ankle sprains, highlights the need for innovative solutions in physical rehabilitation. According to the World Health Organization (WHO), approximately 1.71 billion people worldwide suffer from musculoskeletal conditions, which directly affect individuals' mobility and physical functionality [1]. Among these conditions, lateral ankle sprains stand out due to their high frequency, particularly in sports activities involving abrupt changes in direction, such as football and basketball [2].

In the United Kingdom, ankle sprains account for approximately 5% of emergency room visits [2], and in the United States, nearly 30,000 cases are reported daily [3]. However, these figures may be underestimated, as many individuals do not seek formal medical care for this type of injury [3]. Epidemiological studies show that between 15% and 40% of all sports injuries are ankle sprains, and around 80% are lateral sprains [4].

Various technologies have been developed to address the rehabilitation of these injuries, including exoskeletons [5], orthotic devices [6], and wearable sensors. Each offers specific advantages: exoskeletons provide active movement support [7]; orthoses enable passive joint stabilization; and sensors allow real-time monitoring of the recovery process [8]. However, many of these approaches are limited in portability, precision, or the ability to accurately replicate the physiological motions of the ankle joint [9].

In this context, parallel mechanisms have emerged as a promising alternative [10]. Their structural rigidity and ability to operate with multiple degrees of freedom make them ideal for accurately replicating complex human joint motions [9], [11]. Ankle sprains are among the most common musculoskeletal injuries worldwide, especially among active individuals and athletes [9], [11], [13]. Sudden movements or directional changes during physical activity generate high-risk conditions, particularly when the ankle is subjected to forced inversion or eversion [2]. Due to their high incidence, these injuries are a significant cause of medical consultations in health services. They result in considerable functional limitations, underlining the need for specialized and effective rehabilitation interventions [3].

In Peru, ankle sprains also represent a significant portion of sports-related injuries. According to EsSalud [14], approximately 20% of consultations related to sports trauma are due to ankle sprains, with 80% of these being lateral [10]. Additionally, the 2023 Statistical Bulletin from the National Superintendence of Health (SUSALUD) confirms the recurring nature of ankle sprain consultations in public health services, indicating their high prevalence among the Peruvian population [15].

Despite advancements in rehabilitation technologies, there remains a lack of studies integrating advanced inverse kinematics and screw theory models specifically applied to the human ankle particularly in the design of 3UPS type parallel mechanisms. Moreover, many existing studies do not incorporate a comprehensive analysis of the mechanism's workspace or singularities, which are critical for ensuring stability and effectiveness during clinical operation.

Therefore, this study aims to design and develop a 3UPS parallel mechanism for passively rehabilitating lateral ankle sprains in athletes. The proposed device seeks to precisely replicate the physiological movements of the ankle, maintain a lightweight and portable structure for clinical and home use, and ensure stable operation through analysis of workspace and singular configurations.

This proposal is expected to reduce injury recurrence rates, improve joint stability, and prevent long-term complications such as functional ankle instability or post-traumatic osteoarthritis [12].

II. Background

Parallel mechanisms have been widely studied due to their ability to replicate complex movements with high precision and structural rigidity. According to Merlet, these systems are particularly effective in applications requiring stability and control, such as motion simulators, robot-assisted surgery, and biomechanical training platforms [16]. In rehabilitation, parallel mechanisms have been increasingly used to simulate physiological joint movements accurately and repeatedly.

A. Applications and Design

Parallel mechanisms are known for their precision in replicating joint motions. Wu and Qin [17] developed a 3RRS mechanism that executes compound and straightforward movements, achieving a maximum angular error of 2° in virtual simulations. Despite its effectiveness, the design lacks portability, limiting its applicability in sports or outpatient settings.

Cerna Soto [18], in a design focused on the Peruvian population, presented a 2UPU mechanism suitable for active and passive rehabilitation. However, its movement range is limited to 30° in flexion and 18° in eversion, which constrains its effectiveness in comprehensive ankle therapy.

From a clinical perspective, Barrett Podiatry [19] evaluated customized orthotic devices through biomechanical analysis, emphasizing the importance of tailoring treatment to each patient's anatomical characteristics to enhance joint stability and reduce injury recurrence.

Using the virtual work principle, Abarca Pino [20] proposed a dynamic model for a prosthetic ankle. The simulation validated dorsiflexion and inversion movements with 75.76% accuracy. Nonetheless, the model exhibited time delays in actuator response, highlighting the need for improvements to enable more complex motion control.

B. Modeling and Validation Methods

Kinematic and dynamic modeling are fundamental to optimizing the design of parallel mechanisms. González [21] proposed a dynamic model for a 3UPS mechanism focused on ankle rehabilitation, demonstrating its ability to replicate key joint movements with an error margin below 5% and adaptability for passive therapy.

Similarly, Martínez [22] used MatLab and Simulink to model a 3RRS mechanism for ankle rehabilitation. This achieved accurate simulation of complex joint motions and adaptability to user-specific anatomical variations, contributing to safer and more effective therapy.

López [23] validated a 3UPU mechanism through CAD simulations for dorsiflexion, inversion, and eversion. While adaptable to different anatomies, the design lacked physical validation to confirm clinical applicability.

García [24] developed a 3D model in SolidWorks for a 3UPS mechanism and evaluated its structural resistance under varying loads. Although the design proved feasible for rehabilitation purposes, the validation remained limited to simulation.

Most reviewed studies present significant limitations: limited experimental validation, restricted motion ranges compared to full physiological ankle values, inadequate customization to anatomical variations, and the absence of singularity or workspace analysis. These limitations affect the devices' safety, precision, and clinical applicability.

III. Methodology

A. Mathematical Domain

The mathematical domain comprises the set of equations and formulations required to analyze the 3UPS parallel mechanism comprehensively. This includes the forward and inverse kinematic models, essential to describing the system's behavior, and the expressions that define its workspace and allow the mobile platform to identify reachable configurations. Additionally, the equations related to singularity analysis are incorporated, as they are key to detecting critical configurations in which the system may lose control or stability.

1) Inverse Kinematics: Since inverse kinematics seeks the joint values for the mechanism to achieve a desired position and orientation, the matrix **R** is defined by the angles ψ, θ, and ϕ, while the vector **p** is defined by the positions x, y, and z. Therefore, the main equation that describes the iii-th leg of the mechanism, from the base point $\mathbf{A_i}$ to the mobile point $\mathbf{B_i}$, is given by:

$$L_i = p + R \cdot B_i - A_i \tag{1}$$

Where $\mathbf{A_i}$ and $\mathbf{B_i}$ are the positions of the universal and spherical joints relative to the fixed and mobile bases, respectively, these positions can be represented in matrix form, where each column corresponds to the position of a joint in Cartesian space. Additionally, R_a and R_b represent the radii of the fixed and mobile bases.

$$\mathbf{A} = \begin{bmatrix} R_a & -\frac{R_a}{2} & -\frac{R_a}{2} \\ 0 & \frac{\sqrt{3}}{2}R_a & -\frac{\sqrt{3}}{2}R_a \\ 0 & 0 & 0 \end{bmatrix} \tag{2}$$

$$\mathbf{B} = \begin{bmatrix} R_b & -\frac{R_b}{2} & -\frac{R_b}{2} \\ 0 & \frac{\sqrt{3}}{2}R_b & -\frac{\sqrt{3}}{2}R_b \\ 0 & 0 & 0 \end{bmatrix} \tag{3}$$

a) Geometric Method: Continuing with the geometric method, it states that the magnitude of the vector describing the i-th leg corresponds to the effective length of the mechanism's leg and, in turn, represents the joint value of each prismatic actuator.

$$L_i = |p + R \cdot B_i - A_i| \tag{4}$$

b) Screw Theory: Continuing with the screw theory, it describes the calculation of the effective length as the projection of the vector LiL_iLi onto the unit direction of the screw associated with the leg. Additionally, the unit direction of the screw $\widehat{\boldsymbol{S}_\iota}$ is defined as the normalized vector L_i .

$$\widehat{\mathbf{S}_\mathbf{i}} = \frac{\mathbf{L_i}}{|\mathbf{L_i}|} \tag{5}$$

$$L_i = \widehat{S}_i \cdot L_i \tag{6}$$

2) Workspace: The workspace analysis of a parallel mechanism is conducted to determine the positions and orientations that the mobile platform can achieve relative to the fixed base. This analysis is essential to ensure that the mechanism's design meets the established functional requirements.

To achieve this, the inverse kinematics is formulated and solved for each possible position and orientation of the mobile platform within a defined range. This involves calculating the lengths of the prismatic actuators based on a set of desired positions and orientations. For each configuration, it is verified that the calculated lengths comply with the physical and geometric constraints of the mechanism.

3) Singularities: Singularity analysis is a fundamental part of the study of parallel mechanisms, as these represent critical configurations where the system loses degrees of freedom or becomes unstable.

To perform this analysis, it is formulated that the determinant of the mechanism's Jacobian matrix equals zero. Since the Jacobian is constructed by taking the partial derivatives of the leg lengths with respect to position and orientation, it can be decoupled into two Jacobians: the position Jacobian and the orientation Jacobian. To determine the singularities of each, the procedure remains the same.

$$\det(\boldsymbol{J}) = 0 \tag{7}$$

IV. Results

A. Functional Requirements

The design of a 3UPS parallel mechanism for passive ankle rehabilitation must meet technical and biomechanical requirements to ensure functionality, safety, and efficacy. The device must respect the ankle's physiological ranges of motion, allowing dorsiflexion-plantarflexion from 30° to -20°, abduction-adduction from 10° to -10°, and eversion-inversion from 20° to -10°, to simulate natural movements and restore joint functionality. Its portability, with a maximum weight of 2.5 kg, facilitates handling in clinics and home settings, improving the patient experience. Additionally, it must support loads of up to 250 N to ensure durability and safety while generating a minimum force of 20 N, sufficient to mobilize the ankle by overcoming tissue resistance without causing discomfort or harm.

B. Mathematical Domain

1) Inverse Kinematics: If we start symbolizing the equation that describes the length vector for the i-th leg of the mechanism, equation (1), we obtain a 3×1 vector with the spatial components of the vector.

$$L_i = \begin{bmatrix} L_{i_x} \\ L_{i_y} \\ L_{i_z} \end{bmatrix} \tag{8}$$

Therefore, for each of the three legs of the mechanism, it is expressed as follows:

$$L_1 = \begin{bmatrix} -R_a + R_b c_\psi c_\theta + p_x \\ R_b s_\psi c_\theta + p_y \\ -R_b s_\theta + p_z \end{bmatrix} \tag{9}$$

$$L_2 = \begin{bmatrix} \frac{R_a}{2} + \frac{\sqrt{3}R_b(s_\phi s_\theta c_\psi - s_\psi c_\phi)}{2} - \frac{R_b c_\psi c_\theta}{2} + p_x \\ -\frac{\sqrt{3}R_a}{2} + \frac{\sqrt{3}R_b(s_\phi s_\psi s_\theta + c_\phi c_\psi)}{2} - \frac{R_b s_\psi c_\theta}{2} + p_y \\ \frac{\sqrt{3}R_b s_\phi c_\theta}{2} + \frac{R_b s_\theta}{2} + p_z \end{bmatrix} \tag{10}$$

$$L_3 = \begin{bmatrix} \frac{R_a}{2} - \frac{\sqrt{3}R_b(s_\phi s_\theta c_\psi - s_\psi c_\phi)}{2} - \frac{R_b c_\psi c_\theta}{2} + p_x \\ \frac{\sqrt{3}R_a}{2} - \frac{\sqrt{3}R_b(s_\phi s_\psi s_\theta + c_\phi c_\psi)}{2} - \frac{R_b s_\psi c_\theta}{2} + p_y \\ -\frac{\sqrt{3}R_b s_\phi c_\theta}{2} + \frac{R_b s_\theta}{2} + p_z \end{bmatrix} \tag{11}$$

a) Geometric Method: Continuing with the Geometric Method, equation (4) is used to obtain the joint values. For each leg, the following is derived:

$$L_1 = \sqrt{L_{1_x}^2 + L_{1_y}^2 + L_{1_z}^2} \tag{12}$$

$$L_2 = \sqrt{L_{2_x}^2 + L_{2_y}^2 + L_{2_z}^2} \tag{13}$$

$$L_3 = \sqrt{L_{3_x}^2 + L_{3_y}^2 + L_{3_z}^2} \tag{14}$$

Additionally, if the equations are expanded, they can be expressed as follows:

$$L_1 = \sqrt{(-R_b\, s_\theta + p_z)^2 + \left(R_b\, s_\psi\, c_\theta + p_y\right)^2} + \sqrt{\left(-R_a + R_b\, c_\psi\, c_\theta + p_x\right)^2} \tag{15}$$

$$L_2 = \sqrt{\left(\frac{R_a}{2} + \frac{\sqrt{3}R_b(s_\phi\, s_\theta\, c_\psi - s_\psi\, c_\phi)}{2} - \frac{R_b\, c_\psi\, c_\theta}{2} + p_x\right)^2} + \sqrt{\left(-\frac{\sqrt{3}R_a}{2} + \frac{\sqrt{3}R_b(s_\phi\, s_\psi\, s_\theta + c_\phi\, c_\psi)}{2} - \frac{R_b\, s_\psi\, c_\theta}{2} + p_y\right)^2} + \sqrt{\left(\frac{\sqrt{3}R_b\, s_\phi\, c_\theta}{2} + \frac{R_b\, s_\theta}{2} + p_z\right)^2} \tag{16}$$

$$L_3 = \sqrt{\left(\frac{R_a}{2} + \frac{\sqrt{3}R_b(s_\phi\, s_\theta\, c_\psi - s_\psi\, c_\phi)}{2} - \frac{R_b\, c_\psi\, c_\theta}{2} + p_x\right)^2} + \sqrt{\left(-\frac{\sqrt{3}R_a}{2} + \frac{\sqrt{3}R_b(s_\phi\, s_\psi\, s_\theta + c_\phi\, c_\psi)}{2} - \frac{R_b\, s_\psi\, c_\theta}{2} + p_y\right)^2} + \sqrt{\left(\frac{\sqrt{3}R_b\, s_\phi\, c_\theta}{2} + \frac{R_b\, s_\theta}{2} + p_z\right)^2} \tag{17}$$

b) Screw Theory: For Screw Theory, the unit screw direction of each leg must first be determined, equation (5), which takes the following form:

$$\widehat{\boldsymbol{S_1}} = \begin{bmatrix} \frac{-R_a+R_b c_\psi c_\theta+p_x}{\sqrt{(-R_b s_\theta+p_z)^2+(R_b s_\psi c_\theta+p_y)^2+(-R_a+R_b c_\psi c_\theta+p_x)^2}} \\ \frac{R_b s_\psi c_\theta+p_y}{\sqrt{(-R_b s_\theta+p_z)^2+(R_b s_\psi c_\theta+p_y)^2+(-R_a+R_b c_\psi c_\theta+p_x)^2}} \\ \frac{-R_b s_\theta+p_z}{\sqrt{(-R_b s_\theta+p_z)^2+(R_b s_\psi c_\theta+p_y)^2+(-R_a+R_b c_\psi c_\theta+p_x)^2}} \end{bmatrix} \quad (18)$$

$$\widehat{\boldsymbol{S_2}} = \begin{bmatrix} \frac{\frac{R_a}{2}+\frac{\sqrt{3}R_b\left(s_\phi s_\theta c_\psi - s_\psi c_\phi\right)}{2}-\frac{R_b c_\psi c_\theta}{2}+p_x}{\sqrt{A+B+C}} \\ \frac{-\frac{\sqrt{3}R_a}{2}+\frac{\sqrt{3}R_b\left(s_\phi s_\psi s_\theta + c_\phi c_\psi\right)}{2}-\frac{R_b s_\psi c_\theta}{2}+p_y}{\sqrt{A+B+C}} \\ \frac{\frac{\sqrt{3}R_b s_\phi c_\theta}{2}+\frac{R_b s_\theta}{2}+p_z}{\sqrt{A+B+C}} \end{bmatrix} \quad (19)$$

$$\widehat{\boldsymbol{S_3}} = \begin{bmatrix} \frac{-R_a+R_b c_\psi c_\theta+p_x}{\sqrt{D+E+F}} \\ \frac{R_b s_\psi c_\theta+p_y}{\sqrt{D+E+F}} \\ \frac{-R_b s_\theta+p_z}{\sqrt{D+E+F}} \end{bmatrix} \quad (20)$$

Where each variable represents:

$$A = \left(\frac{\sqrt{3}R_b s_\theta c_\theta}{2}+\frac{R_b s_\theta}{2}+p_z\right)^2$$

$$B = \left(\frac{R_a}{2}+\frac{\sqrt{3}R_b\left(s_\phi s_\theta c_\psi - s_\psi c_\phi\right)}{2}-\frac{R_b c_\psi c_\theta}{2}+p_x\right)^2$$

$$C = \left(-\frac{\sqrt{3}R_a}{2}+\frac{\sqrt{3}R_b\left(s_\phi s_\psi s_\theta + c_\phi c_\psi\right)}{2}-\frac{R_b s_\psi c_\theta}{2}+p_y\right)^2$$

$$D = \left(-\frac{\sqrt{3}R_b s_\phi c_\theta}{2}+\frac{R_b s_\theta}{2}+p_z\right)^2$$

$$E = \left(\frac{R_a}{2}-\frac{\sqrt{3}R_b\left(s_\phi s_\theta c_\psi - s_\psi c_\phi\right)}{2}-\frac{R_b c_\psi c_\theta}{2}+p_x\right)^2$$

$$F = \left(\frac{\sqrt{3}R_a}{2}-\frac{\sqrt{3}R_b\left(s_\phi s_\psi s_\theta + c_\phi c_\psi\right)}{2}-\frac{R_b s_\psi c_\theta}{2}+p_y\right)^2$$

Therefore, the effective length, equation (6), can be calculated using the previous equations, equations (18), (19), and (20). The result is:

$$L_1 = \frac{(-R_b s_\theta+p_z)^2}{\sqrt{(-R_b s_\theta+p_z)^2+(R_b s_\psi c_\theta+p_y)^2+(-R_a+R_b c_\psi c_\theta+p_x)^2}} + \frac{(R_b s_\psi c_\theta+p_y)^2}{\sqrt{(-R_b s_\theta+p_z)^2+(R_b s_\psi c_\theta+p_y)^2+(-R_a+R_b c_\psi c_\theta+p_x)^2}} + \frac{(-R_a+R_b c_\psi c_\theta+p_x)^2}{\sqrt{(-R_b s_\theta+p_z)^2+(R_b s_\psi c_\theta+p_y)^2+(-R_a+R_b c_\psi c_\theta+p_x)^2}} \quad (21)$$

$$L_2 = \frac{\left(\frac{\sqrt{3}R_b s_\phi c_\theta}{2}+\frac{R_b s_\theta}{2}+p_z\right)^2}{\sqrt{A+B+C}} + \frac{\left(-\frac{\sqrt{3}R_a}{2}+\frac{\sqrt{3}R_b\left(s_\phi s_\psi s_\theta + c_\phi c_\psi\right)}{2}-\frac{R_b s_\psi c_\theta}{2}+p_y\right)^2}{\sqrt{A+B+C}} + \frac{\left(\frac{R_a}{2}+\frac{\sqrt{3}R_b\left(s_\phi s_\theta c_\psi - s_\psi c_\phi\right)}{2}-\frac{R_b c_\psi c_\theta}{2}+p_x\right)^2}{\sqrt{A+B+C}} \quad (22)$$

$$L_3 = \frac{(-R_b s_\theta+p_z)\left(-\frac{\sqrt{3}R_b s_\phi c_\theta}{2}+\frac{R_b s_\theta}{2}+p_z\right)}{\sqrt{(-R_b s_\theta+p_z)^2+(R_b s_\psi c_\theta+p_y)^2+(-R_a+R_b c_\psi c_\theta+p_x)^2}} + \frac{(R_b s_\psi c_\theta+p_y)\left(\frac{\sqrt{3}R_a}{2}-\frac{\sqrt{3}R_b\left(s_\phi s_\psi s_\theta+c_\phi c_\psi\right)}{2}-\frac{R_b s_\psi c_\theta}{2}+p_y\right)}{\sqrt{(-R_b s_\theta+p_z)^2+(R_b s_\psi c_\theta+p_y)^2+(-R_a+R_b c_\psi c_\theta+p_x)^2}} + \frac{(-R_a+R_b c_\psi c_\theta+p_x)\left(\frac{R_a}{2}-\frac{\sqrt{3}R_b\left(s_\phi s_\theta c_\psi - s_\psi c_\phi\right)}{2}-\frac{R_b c_\psi c_\theta}{2}+p_x\right)}{\sqrt{(-R_b s_\theta+p_z)^2+(R_b s_\psi c_\theta+p_y)^2+(-R_a+R_b c_\psi c_\theta+p_x)^2}} \quad (23)$$

Where each variable in equation (22) is the same as previously defined.

Finally, an angular sweep can be performed, limited by the range of motion of the ankle, to obtain the leg lengths of the mechanism for both methods.

$$\psi \in [10 \quad -10]^\circ$$
$$\theta \in [30 \quad -20]^\circ$$
$$\phi \in [20 \quad -10]^\circ$$

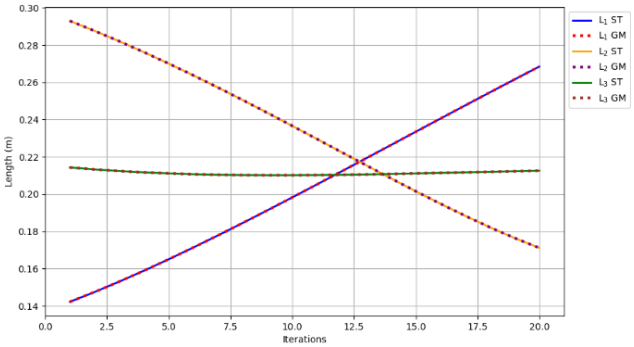

Fig. 1. Angular Sweep of the Geometric Method and Screw Theory.

In Fig. 1, it can be observed that the solid lines represent the result of the Geometric Method, while the dotted lines represent the result of Screw Theory. Additionally, as the angular values approach the negative range, L_1 begins to decrease, L_2 increases, and L_3 remains virtually constant.

2) Workspace: The maximum and minimum lengths of the actuator that moves the system must first be defined to obtain the workspace. Considering that the actuator length is within a range of [0.165, 0.265] m, the workspace of the mechanism was generated by creating groups of spaced values for the position and orientation of the mechanism. This allowed for the analysis of both the positional and orientational workspace.

a) Positional:

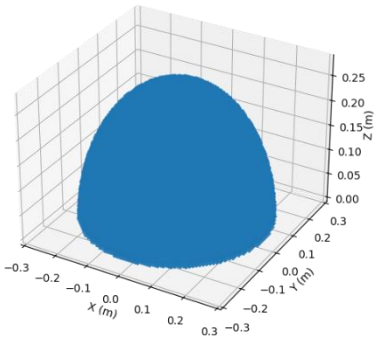

Fig. 2. Positional Workspace.

Only position variables are assigned values for the positional workspace (Fig. 2), so the orientation values are null. The 'x' and 'y' values range from [–0.5, 0.5] m, while the 'z' values range from [0, 1] m with a step of 150.

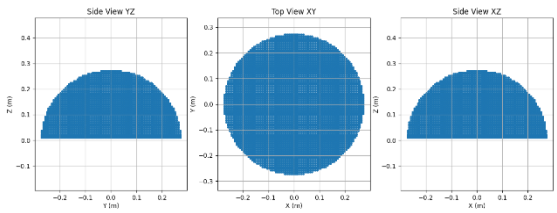

Fig. 3. Views of the Positional Workspace.

The workspace views (Fig. 3) help show the boundaries of the workspace. The Z-axis's maximum height is 0.2717 m, and the minimum is 0.01 m. Meanwhile, on the X and Y axes, the maximum is 0.2718 m, and the minimum is –0.2718 m.

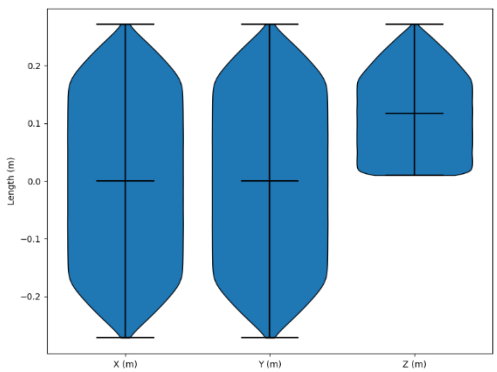

Fig. 4. Violin Plot of the Positional Workspace.

Fig. 4 shows that the X and Y axes have identical distributions, with higher density in the center, which decreases as it approaches the boundaries. However, the Z-axis has a high density at the lower limit, while at the upper limit, it decreases. This is due to the hemispherical shape of the positional workspace.

b) Orientational:

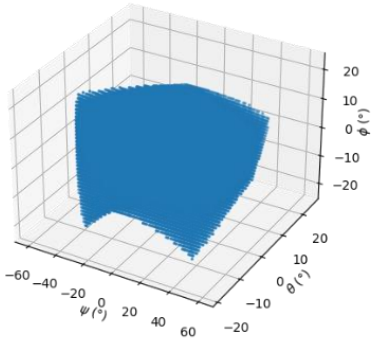

Fig. 5. Orientational Workspace.

In Fig. 5, only the orientation variables are assigned values for the orientational workspace, meaning the position values are set to the home or base state. The psi, zeta, and fi values range from [-90, 90]° with a step size 150.

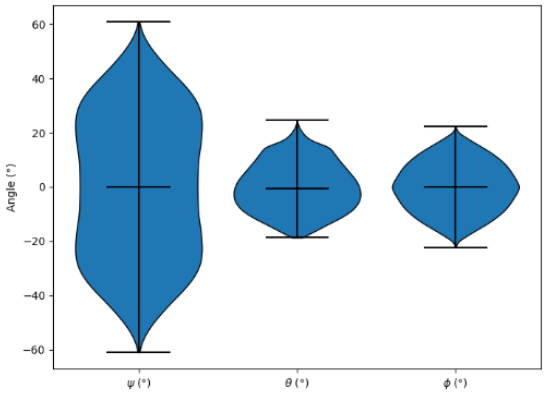

Fig. 6. Violin Plot of the Orientational Workspace.

The violin plot (Fig. 6) helps observe the workspace limits. For psi, the range is from 61.0067° to -61.0067°; for zeta, from 24.7651° to -18.7248°; and for ϕ, from 22.349° to -22.349°. Additionally, there is a higher concentration of reachable angles in the center.

3) Singularities: To obtain the system's singularities, the determinant of the mechanism's Jacobian must be set to zero. This results in a fractional equation with six unknowns, three for position and three for orientation. Additionally, the denominator can be excluded to simplify the analysis since it cannot be zero to avoid indeterminacy, and the focus is placed on the numerator.

a) Posicional:

$$6{R_a}^2(x\,s_\phi\,s_\psi + x\,s_\theta\,c_\phi\,c_\psi - x\,s_\theta - y\,s_\phi\,c_\psi + y\,s_\phi\,c_\theta + y\,s_\psi\,s_\theta\,c_\phi - z\,s_\phi\,s_\psi\,s_\theta - z\,c_\phi\,c_\psi + z\,c_\phi\,c_\theta - z\,c_\psi\,c_\theta + z) \quad (24)$$

The equation (24) can be analyzed for orientation angular values, which, for simplicity in analysis, can take values of 0º, 90º, 180º, or 270º, as they are contained within sine and cosine functions.

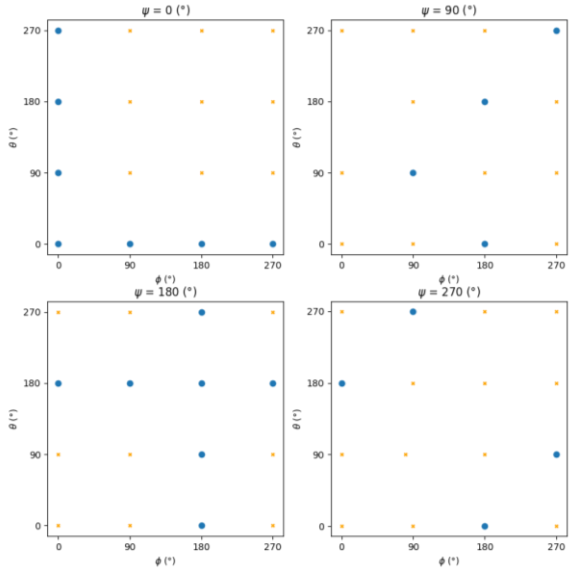

Fig. 7. Total position singularities of the mechanism.

From Fig. 7, it can be observed that there are 22 singular position configurations for the mechanism. However, caution must be taken with these. If we observe the graph for $\psi = 0°$, singularities occur when this angle, along with θ and ϕ , are equal to zero. However, this configuration corresponds to the rest or "home" position. Furthermore, there is a possibility that two sets of angles result in the same posture for the mechanism. Therefore, it is necessary to scrutinize the sets of singular values.

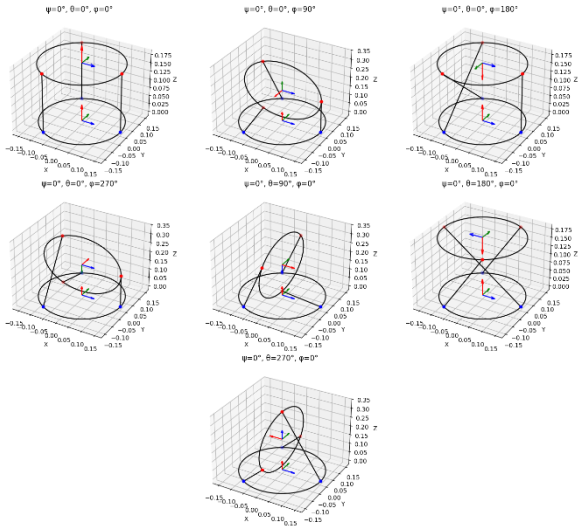

Fig. 8. Position singularities of the mechanism for $\psi = 0°$.

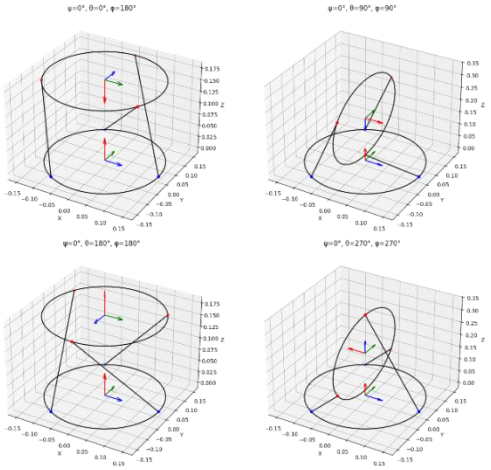

Fig. 9. Position singularities of the mechanism for $\psi = 90°$.

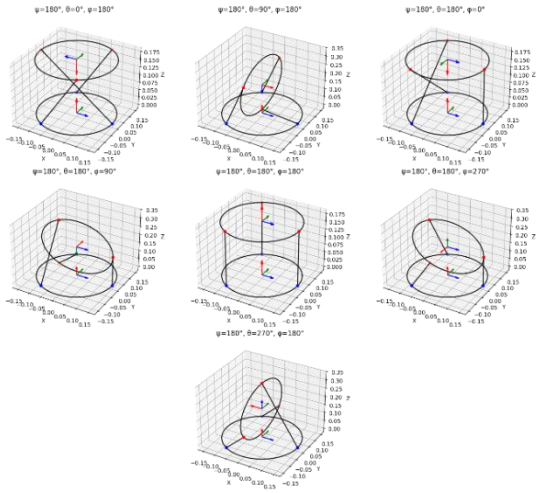

Fig. 10. Position singularities of the mechanism for $\psi = 180°$.

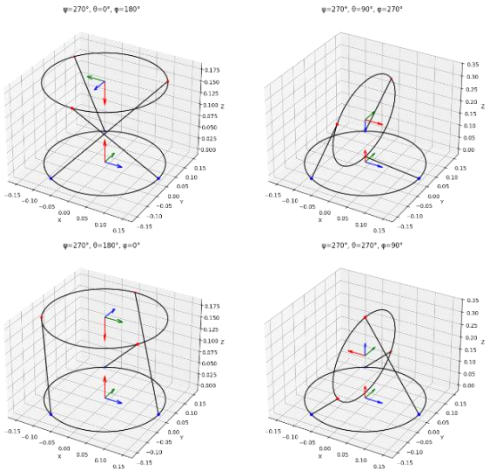

Fig. 11. Position singularities of the mechanism for $\psi = 270°$.

Upon inspecting the graphs, Fig. 8, 9, 10, and 11, it can be observed that out of the 22 singularities, several postures repeat for at least two sets of values. Therefore, the number of singular postures is reduced to 12. Additionally, postures where two orientation variables are zero can be written in another way. Below are the configurations, their sets of angles, and their equivalents, if applicable.

TABLE I
Position singularities of the mechanism.

Conf.	Set 1(°)	Set 2(°)	Set 3(°)
1	[0, 0, 0]	[180, 180, 180]	
2	[0, 0, 90]	[180, 180, 270]	
3	[0, 0, 180]	[180, 180, 0]	
4	[0, 0, 270]	[180, 180, 90]	
5	[0, 90, 0]	[180, 90, 180]	[90, 90, 90]
6	[0, 180, 0]	[180, 0, 180]	
7	[0, 270, 0]	[180, 270, 180]	[90, 270, 270]
8	[90, 0, 180]	[270, 180, 0]	
9	[90, 180, 180]		
10	[270, 0, 180]		
11	[270, 90, 180]		
12	[270, 180, 90]		

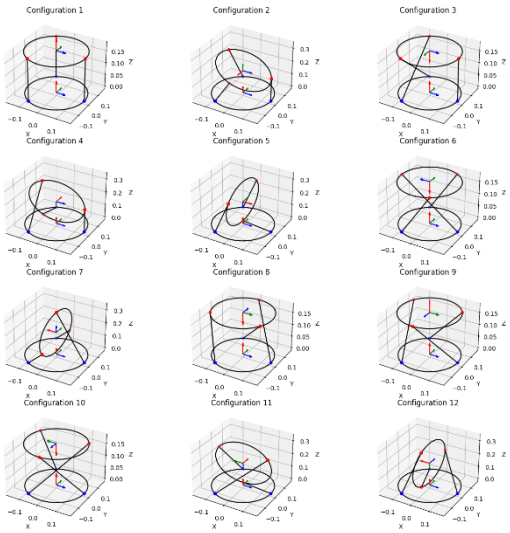

Fig. 12. Position singularities of the mechanism.

b) Orientational:

$$
\begin{aligned}
&3\sqrt{3}RaRb^3c_\theta(R_a^2s_\phi^2s_\psi c_\theta - R_a^2s_\phi s_\theta c_\psi \\
&+R_a^2s_\psi s_\theta^2 + R_axs_\phi^2s_\psi c_\theta + R_axs_\phi s_\theta c_\psi \\
&-R_axs_\psi s_\theta^2c_\phi + R_ays_\phi^2c_\psi c_\theta - R_ays_\phi s_\psi s_\theta \\
&-R_ays_\theta^2c_\phi c_\psi - 4R_azs_\phi^2s_\psi s_\theta c_\psi - 2yzs_\phi^2s_\theta \\
&+2R_azs_\phi s_\psi^2s_\theta^2c_\phi + 2R_azs_\phi s_\psi^2c_\phi - 2R_azs_\phi s_\psi^2c_\theta \\
&-R_azs_\phi s_\theta^2c_\phi + 2R_azs_\phi s_\psi^2c_\phi - \frac{R_azs_{2\phi}}{2} \\
&-2x^2s_\phi^2s_\psi c_\theta + 2xys_\phi^2c_\psi c_\theta - 2xys_\phi s_\psi s_\theta \\
&-2xys_\theta^2c_\phi c_\psi + 4xzs_\phi^2s_\psi s_\theta c_\psi + 4xzs_\phi s_\theta^2c_\phi \\
&-2xzs_\phi s_\psi^2s_\theta^2c_\phi - 2xzs_\phi s_\psi^2c_\phi - 2xzs_\phi s_\psi^2c_\theta \\
&-xzs_{2\phi} + 2y^2s_\phi s_\theta c_\psi - 2y^2s_\psi s_\theta^2c_\phi \\
&+4yzs_\phi^2s_\psi^2s_\theta + 2yzs_\phi s_\psi s_\theta^2c_\phi c_\psi \\
&+2yzs_\phi s_\psi c_\psi c_\theta - 2yzs_\psi^2s_\theta c_\phi c_\theta \\
&-2yzs_\psi^2s_\theta + 2z^2s_\phi^2s_\psi c_\theta + 2z^2s_\psi s_\theta^2c_\phi \\
&-2z^2s_\psi c_\phi - 2z^2s_\psi c_\theta \\
&+G + H - I - J - K - M \\
&-N + Q - T + U + V - W)
\end{aligned}
\tag{25}
$$

$$G = \frac{R_a^2\left(c_{-2\phi+\psi+2\theta} - c_{2\phi-\psi+2\theta} + c_{2\phi+\psi-2\theta} - c_{2\phi+\psi+2\theta}\right)}{16}$$

$$H = \frac{R_ax\left(c_{-2\phi+\psi+2\theta} - c_{2\phi-\psi+2\theta} + c_{2\phi+\psi-2\theta} - c_{2\phi+\psi+2\theta}\right)}{16}$$

$$I = \frac{R_ay\left(s_{-2\phi+\psi+2\theta} + s_{2\phi-\psi+2\theta} + s_{2\phi+\psi-2\theta} - s_{2\phi+\psi+2\theta}\right)}{16}$$

$$J = \frac{R_az\left(-c_{-\phi+2\psi+2\theta} + c_{\phi-2\psi+2\theta} + c_{\phi+2\psi-2\theta} - c_{\phi+2\psi+2\theta}\right)}{8}$$

$$K = \frac{x^2\left(c_{-2\phi+\psi+2\theta} - c_{2\phi-\psi+2\theta} + c_{2\phi+\psi-2\theta} - c_{2\phi+\psi+2\theta}\right)}{8}$$

$$M = \frac{xy\left(s_{-2\phi+\psi+2\theta} + s_{2\phi-\psi+2\theta} + s_{2\phi+\psi-2\theta} - s_{2\phi+\psi+2\theta}\right)}{8}$$

$$N = \frac{xz\left(-c_{-\phi+2\psi+2\theta} + c_{\phi-2\psi+2\theta} + c_{\phi+2\psi-2\theta} - c_{\phi+2\psi+2\theta}\right)}{8}$$

$$Q = \frac{z^2\left(c_{-2\phi+\psi+2\theta} - c_{2\phi-\psi+2\theta} + c_{2\phi+\psi-2\theta} - c_{2\phi+\psi+2\theta}\right)}{8}$$

$$T = \frac{yz\left(-s_{\phi-2\theta} + s_{\phi+2\theta}\right)}{2}$$

$$U = \frac{yz\left(c_{2\phi-2\psi} - c_{2\phi+2\psi}\right)}{4}$$

$$V = \frac{R_az\left(c_{2\psi-\theta} - c_{2\psi+\theta}\right)}{2}$$

$$W = \frac{xz\left(c_{2\psi-\theta} - c_{2\psi+\theta}\right)}{2}$$

The equation (25) can be analyzed for the angular orientation values, which, for ease of analysis, can take the values of 0º, 90º, 180º, or 270º, since these values are included in the sine and cosine functions.

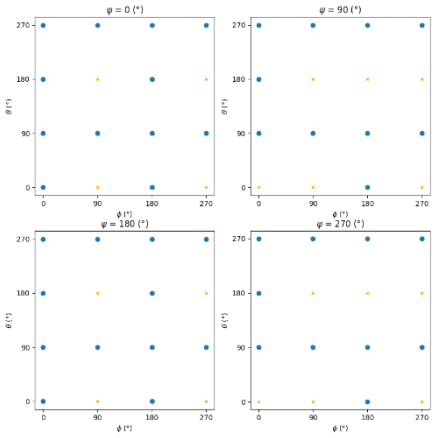

Fig. 13. Total orientational singularities of the mechanism.

From Fig. 13, there are 44 singular position configurations for the mechanism. However, caution must be taken with these. If we observe the graph for $\psi = 0°$, singularities occur when this angle, along with θ and ϕ , are equal to zero. However, this

configuration corresponds to the rest or "home" position. Furthermore, there is a possibility that two sets of angles result in the same posture for the mechanism. Therefore, it is necessary to scrutinize the sets of singular values.

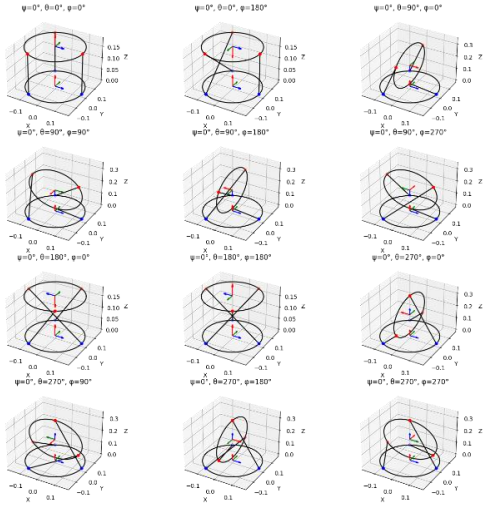

Fig. 14. Orientational singularities of the mechanism for $\psi = 0°$.

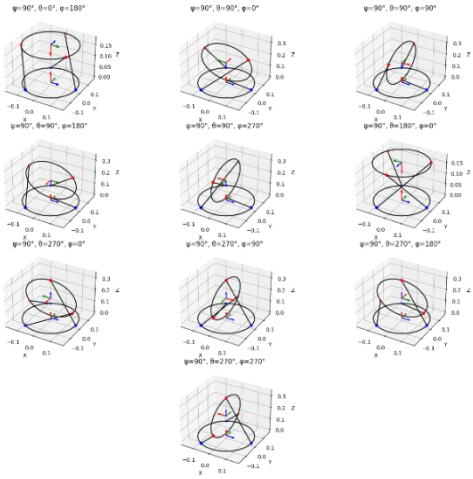

Fig. 15. Orientational singularities of the mechanism for $\psi = 90°$.

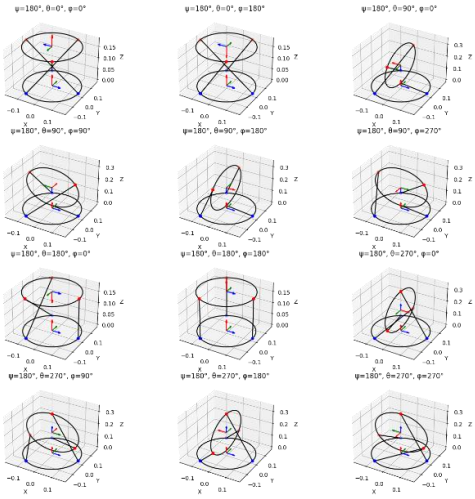

Fig. 16. Orientational singularities of the mechanism for $\psi = 180°$.

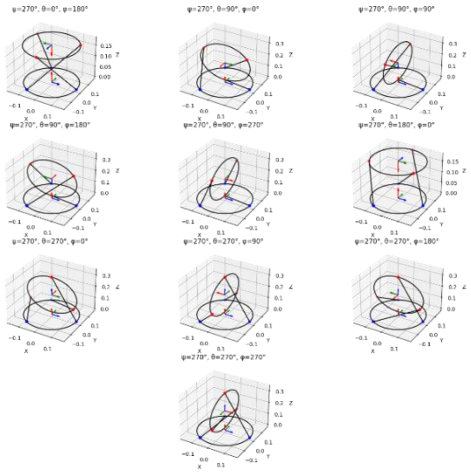

Fig. 17. Orientational singularities of the mechanism for $\psi = 270°$.

Upon inspecting the graphs, Figs. Several postures repeat for at least two sets of values in 14, 15, 16, and 17 out of the 44 singularities. Therefore, the number of singular postures is reduced to 14. Additionally, postures where two orientation variables are zeros can be written in another way. Below are the configurations, the sets of angles, and their equivalents, if applicable.

TABLE II
Orientational singularities of the mechanism.

Conf.	Set 1(°)	Set 2(°)	Set 3(°)	Set 4(°)
1	[0, 0, 0]	[180, 180, 180]		
2	[0, 0, 180]	[180, 180, 0]		
3	[0, 180, 0]	[180, 0, 180]		
4	[0, 180, 180]	[180, 0, 0]		
5	[90, 0, 180]	[270, 180, 0]		
6	[90, 180, 0]	[270, 0, 180]		
7	[0, 90, 0]	[180, 90, 180]	[90, 90, 90]	[270, 90, 270]
8	[0, 90, 90]	[180, 90, 270]	[90, 90, 180]	[270, 90, 0]
9	[0, 90, 180]	[180, 90, 0]	[90, 90, 270]	[270, 90, 90]
10	[0, 90, 270]	[180, 90, 90]	[90, 90, 0]	[270, 90, 180]
11	[0, 270, 180]	[180, 270, 270]	[90, 270, 270]	[270, 270, 90]
12	[0, 270, 90]	[180, 270, 0]	[90, 270, 0]	[270, 270, 180]
13	[0, 270, 90]	[180, 270, 90]	[90, 270, 90]	[270, 270, 270]
14	[0, 270, 90]	[180, 270, 180]	[90, 270, 180]	[270, 270, 0]

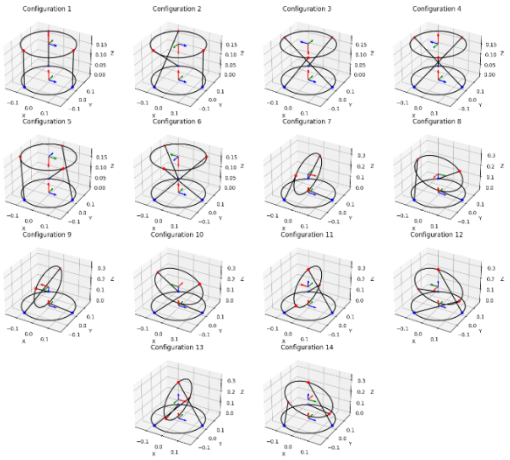

Fig. 18. Orientational singularities of the mechanism.

V. Conclusions

The inverse kinematics was developed using two complementary approaches, the geometric method and screw theory. Both methods allow for the derivation of the necessary equations to determine the joint configurations of the mechanism. The results obtained from both methods show a remarkable similarity between the equations derived, as they share similar structures and lead to equivalent solutions for the joint configurations of the mechanism.

On the other hand, the workspace of the mechanism fully meets the required physiological movement ranges of the ankle for rehabilitation. The positional workspace has a displacement range along the X, Y, and Z axes, allowing mobility for desired configurations. Meanwhile, the orientational workspace covers the angles of flexion-extension, abduction-adduction, and eversion-inversion movements for the angles ψ, θ, and ϕ, respectively, within biomechanically safe limits.

Finally, the singularity analysis conducted on the mechanism helps identify and determine the critical configurations that could compromise the system. Initially, 22 singular positional configurations were found, which were reduced to 12 postures. Likewise, 44 singular orientational configurations were found, which were reduced to 14 postures after eliminating redundancies and considering equivalences between sets of angles. Additionally, all singular configurations lie outside the mechanism's workspace, and the one defined for the ankle's movement ranges.

References

[1] World Health Organization, "Musculoskeletal disorders," *World Health Organization*, online. Available: https://www.who.int/news-room/fact-sheets/detail/musculoskeletal-conditions. [Accessed: Sep. 15, 2024].

[2] T. Bestwick-Stevenson, L. A. Wyatt, D. Palmer, R. M. Smith, and C. J. Jones, "Incidence and risk factors for poor ankle functional recovery, and the development and progression of posttraumatic ankle osteoarthritis after significant ankle ligament injury (SALI): the SALI cohort study protocol," *BMC Musculoskeletal Disorders*, vol. 22, p. 362, 2021, doi: https://doi.org/10.1186/s12891-021-04230-8.

[3] G. J. Cavazos Jr. and L. B. Harkless, "Epidemiology of ankle sprains and the role of sports medicine in their management," *Journal of Sports Medicine and Therapy*, vol. 5, no. 1, pp. 1-7, 2020. [Online]. Available: https://www.heighpubs.org/jsmt/jsmt-aid1052.php.

[4] N. Bsoul, L. Ning, L. Cai, S. Ahmed, and H. Lee, "Evidence-based clinical practice guidelines for the management of acute ankle injuries according to a PRISMA systematic review and quality appraisal with AGREE II," BMC *Musculoskeletal Disorders*, vol. 25, p. 523, 2024, doi: https://doi.org/10.1186/s12891-024-07655-z.

[5] R. F. Asto-Bonifacio, D. Parco-Llorona, H. Valcarcel-Castillo, C. A. Rojas-Vergara, and D. Huamanchahua, "Electronic design of Knee and Ankle Exoskeleton for Motor Rehabilitation of Soccer Athletes," *2023 IEEE Colombian Caribbean Conference (C3)*, Barranquilla, Colombia pp. 1-6, 2023.

[6] D. Huamanchahua, A. A. Alarcón-Vera and S. A. Seminario-Valdiviezo, "Prototype Knee Orthosis for Anterior Cruciate Ligament Rupture in Ball Sports Athletes," *2022 IEEE 13th Annual Ubiquitous Computing, Electronics & Mobile Communication Conference (UEMCON)*, New York, NY, NY, USA, pp. 0230-0237, 2022.

[7] D. Huamanchahua, C. L. Otarola-Ruiz, A. Quispe-Piña and E. J. De La Torre-Velarde, "Knee and Ankle Exoskeletons for Motor Rehabilitation: A Technology Review," *2022 IEEE International IOT, Electronics and Mechatronics Conference (IEMTRONICS)*, Toronto, ON, Canada, pp. 1-7, 2022.

[8] H. Böhm and M. Hösl, "Effectiveness of ankle-foot orthoses in the treatment of foot drop after stroke: A review of the literature," *Journal of Rehabilitation Medicine*, vol. 42, no. 7, pp. 579-585, 2010, doi: 10.2340/16501977-0574.

[9] L. H. Wright, T. W. Linens, and J. W. Cain, "Risk Factors for Lateral Ankle Sprains and Chronic Ankle Instability," *J. Athl. Train.*, vol. 54, no. 6, pp. 611-621, 2019. [Online]. Available: https://meridian.allenpress.com/jat/article/54/6/611/420866.

[10] D. Huamanchahua, A. Tadeo-Gabriel, R. Chávez-Raraz and K. Serrano-Guzmán, "Parallel Robots in Rehabilitation and Assistance: A Systematic Review," *2021 IEEE 12th Annual Ubiquitous Computing, Electronics & Mobile Communication Conference (UEMCON)*, New York, NY, USA, pp. 0692-0698, 2021.

[11] K. D. Roos, J. Kerkhoffs, and R. J. de Bie, "What Is 'Best Practice' for Acute Ankle Sprains?" *Br. J. Sports Med.*, vol. 50, no. 24, pp. 1496-1498, 2016. [Online]. Available: https://bjsm.bmj.com/content/50/24/1496.

[12] IMSS, "UMAE Traumatology, Orthopedics, and Rehabilitation of IMSS handles over 138,000 emergencies in 2023," *Closer to the Citizen IMSS*, Sep. 2023. [Online]. Available: https://imss.gob.mx.

[13] C. Doherty, E. Delahunt, B. Caulfield, J. Doody, M. Harty, and K. McKeon, "The Incidence and Prevalence of Ankle Sprain Injury: A Systematic Review and Meta-Analysis of Prospective Epidemiological Studies," *Sports Med.*, vol. 44, pp. 123-140, 2014, doi: https://doi.org/10.1007/s40279-013-0102-5.

[14] A. R. León Villar, "Ankle Sprain," *EsSalud*, May 17, 2022. [Online]. Available: https://hdl.handle.net/20.500.12959/4111. [Accessed: Sep. 21, 2024].

[15] Superintendencia Nacional de Salud (SUSALUD), "Statistical Bulletin 2023," Sep. 1, 2023. [Online]. Available: https://www.gob.pe/institucion/susalud/informes-publicaciones/4595872-boletin-estadistico-2023. [Accessed: Sep. 21, 2024].

[16] J.-P. Merlet, *Parallel Robots*, 2nd ed. Dordrecht, Netherlands: Springer, 2006, doi: 10.1007/1-4020-4133-0.

[17] X. Wu and T. Qin, "Design and Experimental Research of 3-RRS Parallel Ankle Rehabilitation Robot," *Micromachines*, vol. 13, no. 6, pp. 1-15, 2022. [Online]. Available: https://doi.org/10.3390/mi13060950. [Accessed: Oct. 27, 2024].

[18] D. A. Cerna Soto, "Mechanical Design of a Device for Ankle Mobility Rehabilitation Using a Parallel Mechanism," *Undergraduate Thesis*, Pontificia Universidad Católica del Perú, 2020. [Online]. Available: https://hdl.handle.net/20.500.12404/7063. [Accessed: Oct. 27, 2024].

[19] Barrett Podiatry, "Biomechanics," *Barrett Podiatry*, San Antonio, TX, 2023. [Online]. Available: https://barrettpodiatry.com/podiatry-treatment/biomechanics/. [Accessed: Oct. 27, 2024].

[20] V. E. Abarca Pino, "Modeling and Dynamic Simulation of a Parallel Mechanism for a Prosthetic Ankle with 3 Degrees of Freedom," *Undergraduate Thesis*, Pontificia Universidad Católica del Perú, 2024. [Online]. Available: https://hdl.handle.net/20.500.12404/29095. [Accessed: Oct. 27, 2024].

[21] J. González, "Dynamic Modeling of a 3-UPS Parallel Mechanism for Ankle Rehabilitation," *Undergraduate Thesis*, Universidad Nacional Autónoma de México, 2020. [Online]. Available: https://repositorio.unam.mx/thesis/24638. [Accessed: Oct. 27, 2024].

[22] P. Martínez, "Kinematic Analysis of a 3-RRS Mechanism for Ankle Rehabilitation," *Undergraduate Thesis*, Universidad Politécnica de Valencia, 2018. [Online]. Available: https://dspace.upv.es/handle/10251/109359. [Accessed: Oct. 27, 2024].

[23] M. Lopez, "Design and Simulation of a 3-UPU Parallel Mechanism for Ankle Rehabilitation," *Undergraduate Thesis*, University of Michigan, 2021. [Online]. Available: https://psdl-dev.engin.umich.edu/ARThesis2021.pdf. [Accessed: Oct. 27, 2024].

[24] A. García, "3D Modeling of a 3-UPS Parallel Mechanism for Ankle Rehabilitation," *Undergraduate Thesis*, Universidad Técnica de Madrid, 2019. [Online]. Available: https://eprints.upm.es/60852. [Accessed: Oct. 27, 2024].